The FOPI Detector at SIS/GSI

J. Ritman

for the FOPI Collaboration*

Abstract

The FOPI detector system has been assembled at GSI to study the properties of hot and dense nuclear matter. This system which covers nearly the full 4π solid angle has been built in three stages. (1) The forward plastic wall detector was completed in 1990 and has been successfully employed to measure intermediate mass fragment production in reactions of Au on Au at 150 to 1000 $A\cdot$MeV. (2) The superconducting solenoid and Central Drift Chamber were completed in 1992 and have also been successfully employed to study charged pion production in Au on Au at 1050 $A\cdot$MeV. (3) The plastic scintillator/Cherenkov Barrel and forward drift chamber HELITRON are partially installed and the full commissioning is expected at the beginning of 1995. Results from recent test experiments involving all three phases which demonstrate the detector's ability to identify the rare signals from Kaon and Λ particle production will be presented.

1 Introduction

In order to get the most complete event characterization possible of the relativistic heavy ion collisions produced by the Heavy Ion Synchrotron SIS (0.1-2 $A\cdot$GeV) at GSI Darmstadt, the nearly 4π detector system FOPI has been built [1]. The beam energy regime available here spans the range from where nuclear mean-field effects dominate up to the excitation of internal nucleonic degrees of freedom within a sizable fraction of the collisional system. Over this energy regime, the measurable signals from heavy ion collisions include heavy nuclear fragments (up to Z$\sim$20), individual nucleons, and mesons which are produced in the hot and compressed nuclear matter. Because of the large variation in detector requirements for these various particle types, the FOPI system has been built with a modular design where each component has been optimized for the detection of a particular type of particle.

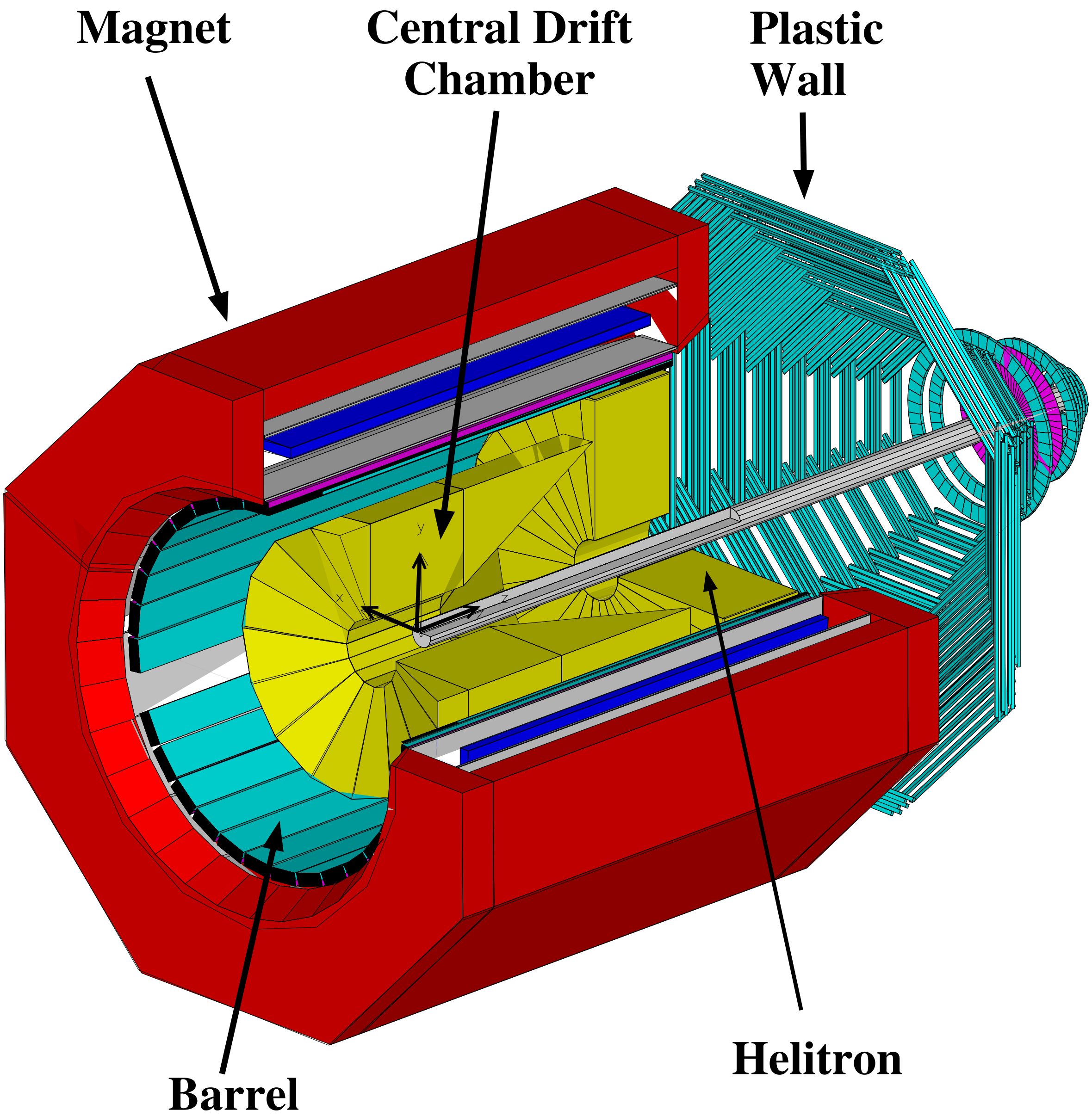

Figure 1: The 4π detector FOPI at GSI. For reference, the 3 arrows at the coordinate system origin are 50 cm long.

The full FOPI detector, shown in figure 1, has been constructed in three stages: The first phase, which was completed in 1990, consists of the Forward Plastic Wall (764 scintillators) and an inner shell of 188 energy loss detectors (not shown). The wall measures the charge and velocity of all charged particles emitted with laboratory polar angles between $1^\circ < \Theta_{Lab} < 30^\circ$ over the full azimuth. The installation in 1992 of the Superconducting Magnet and Central Drift Chamber (CDC) enabled momentum determination of charged particles within an expanded angular range of $30^\circ < \Theta_{Lab} < 150^\circ$. In the final phase, with expected completion in the beginning of 1995, velocity determination by the Scintillator and Cherenkov Barrel will supplement the CDC and the forward drift chamber HELITRON will permit momentum determination down to $\Theta_{Lab} > 7°$.

2 Forward Wall

The main component of the first phase is the Forward Wall which is described in detail in reference [2]. The Forward Wall measures the energy loss (ΔE) and velocity of all charged particles emitted from the reaction zone with laboratory polar angles between $1° < \Theta_{Lab} < 30°$ over the full azimuthal range. The Wall is divided into two polar angular regions. From $1° < \Theta_{Lab} < 7°$ the Zero Degree (ZER) detectors measure the particle velocity and the Rosace measures the energy loss. Above 7° the particle velocity measurements are made by the Plastic Wall (PLAWA) and a large solid angle ionization chamber (Parabola) records ΔE.

The Zero degree system consists of 252 counters produced with Bicron BC 404 scintillating material. The 2 cm thick detector paddles are of trapezoidal shape and are arranged in 7 concentric rings. The light from each paddle is collected in 2" photomultipliers (Philips XP2262) which are shielded with 0.3 mm μmetal cylinders. Individual quartz fibers from the laser calibration and monitoring system are fixed in the center on the rear surface of each paddle. Tests determined the homogeneity of the light output to be about 5% across the detector. The time resolution is limited by this geometry and is between $\sigma_t \approx$ 230-340 ps depending upon the length of the paddle, the amount of primary light, and the location of the hit in the paddle. The signal is first split then the Time of Flight (ToF) and integral charge are recorded with Lecroy Fastbus modules 1875 (TDC) and 1885F (ADC). A graphic display of the amplitude versus the particle velocity for all 252 paddles combined is shown in Fig. 2b.

Charge identification is achieved by exploiting the relationship between the energy loss (dE/dx) and the velocity of ionizing particles passing through matter (i.e. Bethe-Bloch formula). Since the ZER is thick enough to stop slower fragments, the Rosace was installed in front of the ZER to provide dE/dx information for the fragments stopped in the ZER. Each 2 mm thick by 340 mm long paddle is placed radially in a Rosace configuration. The 60 scintillator paddles (NE 102A) are each connected to 3/4" Hamamatsu R2076 phototubes. Because of the trapezoidal shape of each paddle the light output varies up to 8% along the polar direction and up to 15% in the azimuth. A typical ΔE vs velocity plot for a single Rosace paddle (velocity determined by the ZER) is shown in Fig. 2d.

For $7° < \Theta_{lab} < 30°$ the velocity of all charged reaction products is determined by the Outer Plastic Wall (PlaWa). The PlaWa is composed of 512 scintillator strips (Bicron BC 408) grouped into 8 radial sectors. The strips have a cross-section of 24×18 mm and a length that varies between 450 to 1650 mm which are located at a distance between 360 and 440 cm from the target. Philips XP2972/01 1" tubes are

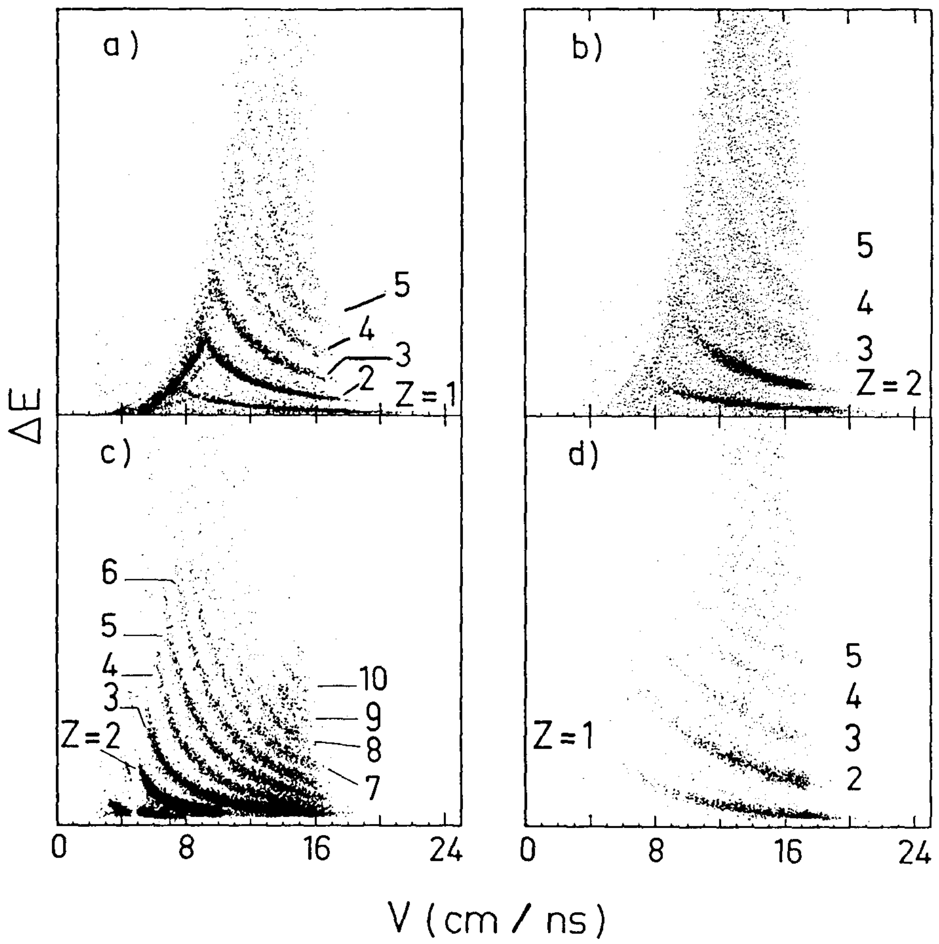

Figure 2: Energy loss versus particle velocity measured in the (a) PlaWa, (b) ZER, (c) Parabola, and (d) Rosace.

mounted on both ends of the strips and a quartz fiber coupled to the back of each strip allows for calibration and monitoring with the laser system. Stray magnetic fields are shielded by 15 cm long and 1 mm thick cylinders of Permenorm 5000S2. Similar to the ZER the PlaWa signals are split so they can be recorded in both an ADC and TDC. By combining the energy and time signals from the tubes on the right and left side of each strip, the quantities ΔE, ToF, and Position(POS) can be determined by the following relations:

$$\Delta E \propto \sqrt{E_L E_R},$$

$$ToF = \frac{1}{2}(T_L + T_R) + Const,$$

$$POS_T \propto \frac{1}{2}(T_L - T_R), \qquad or \qquad POS_E \propto \ln(E_L/E_R).$$

The time resolution of this system has been measured with 44 MeV electrons to be $\sigma_t \approx 80$ ps. The resolution improves to ~ 40 ps for light intensities $10\times$ larger than that of minimum ionizing particles (MIL). Based on a measured effective velocity of the light front in the scintillators $v_{eff} = 15.1$ cm/ns, the position resolution is $\sigma_{POS} \approx 1.2$ cm. Clearly visible in Fig 2a is the "punch-through" point (e.g. near 9.5 cm/ns for He) above which the particles have sufficient energy to pass completely through the detector. Quenching effects are responsible for deviations from a pure $\Delta E \propto Z^2$ dependence.

Since the charge can not be determined for reaction products below the punch-through point, a parabola shaped ionization chamber has been installed to extend the dE/dx information to lower velocities. The Parabola consists of 16 double ionization chambers each with an area between 0.5 and 0.9 m^2 and a thickness of 12 cm. The anode is held at ground while the two cathode planes are subjected to typically -4.8 kV. A mixture of Ar/CH_4 (90/10) is provided with a flow of about 0.3 l/min to operate the chamber at a slight overpressure. Each anode foil is segmented into 8 radial subanodes with $\Delta\phi = 5.6°$. Fig 2c shows the result after combining the ΔE from the Parabola with the velocity from the PlaWa.

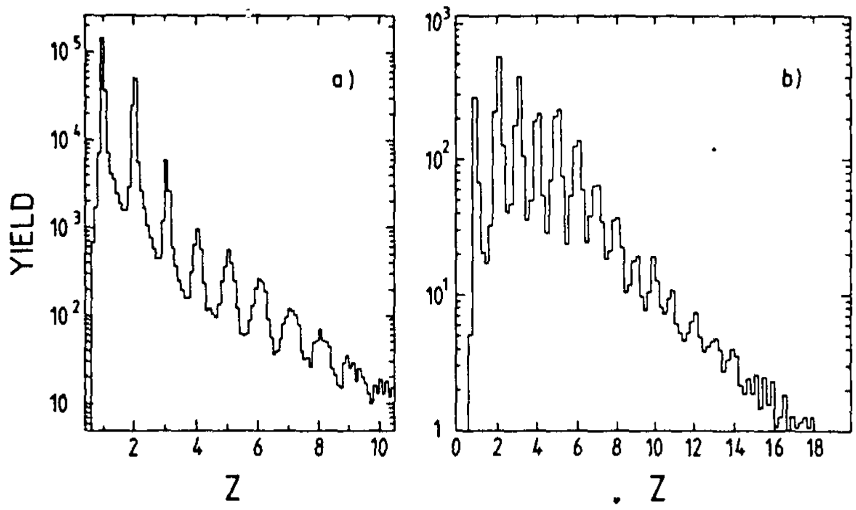

Figure 3: Element spectra produced by a linearization of the data in parts c and d of the previous figure.

After correction for quenching effects, a linearization of the Rosace-ZER and Parabola-PlaWa data is shown in Fig. 3. This system does not provide for isotope determination; therefore, in the data analysis the cluster mass number is assumed to be $A = 2Z$ for all elements heavier than H.

Since installation of the Forward Wall, numerous experiments have been performed. A systematic study of the system Au on Au has been carried out at beam energies ranging from 100 to 1000 A·MeV. Some of the final results from these experiments using the first phase have already been published [3, 4, 5, 6], and further publications are approaching completion. In addition, a number of other experiments have been performed combining the FOPI forward wall with the neutron detector LAND [7] and with the photon spectrometer TAPS [8, 9, 10, 11].

3 Central Drift Chamber

In 1992 a major expansion of the FOPI facility was undertaken by installing the Superconducting Solenoid and the Central Drift Chamber (CDC). The CDC is a drift chamber of the jet type that allows tracking of the paths taken by all charged reaction products emitted in the polar angle range $30° < \Theta_{lab} < 150°$. The flight paths are curved by the magnetic field from the solenoid, therefore (transverse) momentum determination and mass identification of these reaction products is possible.

The Superconducting Solenoid was produced by Oxford with Niobium Titanium/Copper and operates submerged in a bath of liquid Helium. When operating at the maximum current of 720 A a 0.6 T field is produced in the central volume. In this volume the field is homogeneous to $\pm 1.5\%$. With a diameter of 2.4 m and a length of 3.3 m, this is one of the largest existing superconducting solenoids. At full field, this magnet contains over 3.4 MJ stored energy. The coil is housed in a 100 Ton iron yoke which is mounted upon a platform that allows the magnet to be moved with relative ease by applying compressed air.

The CDC is a tracking chamber that covers the full azimuthal angle within the polar angle range $30° < \Theta_{lab} < 150°$. The detector is subdivided into 16 sectors each containing 60 sense wires and 60 potential wires all of which are aligned parallel to the beam axis. The sense wires are resistive and readout on both end, which permits z-coordinate (beam axis) reconstruction of the hit via charge division. The drift electrons have a velocity of about 40 μm/ns so the drift time can be exploited to determine the XY plane position. Since the direction of the drift electrons can not be measured, each hit has a symmetric partner on the other side of the anode plane (mirror hit). Although the mirror hits combine to form mirror tracks, this ambiguity is removed by tilting the wire planes by 8° away from the beam axis. With this design, the mirror tracks can be identified since they do not originate from the target. Furthermore, the wires within a plane are alternately staggered by $\pm 100\mu$m. Not only is this staggering needed for the electrical stability, but it also provides an additional means to identify the mirror tracks. The individual signal wires vary between 86 and 190 cm; and the 30μm thick W-Rh(20%) wire has a resistance of 500 Ω/m. Typically the chamber is operated at a slight overpressure with a mixture of 88% Ar, 10% Isobutene, and 2% CH_4.

In central Au on Au collisions up to 100 particles may be registered per event.

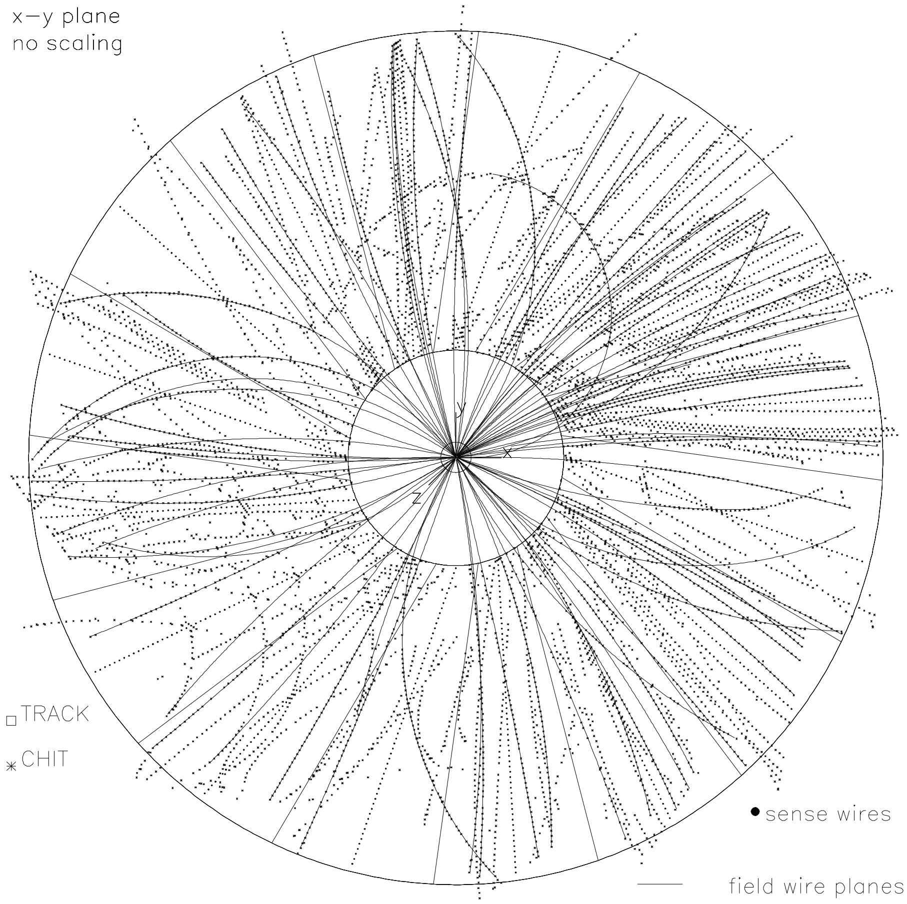

Figure 4: Event Display of a typical Au on Au reaction with 79 particle tracks in the x-y plane of the CDC. The points display the detected hits, the curves present the identified tracks.

With a typical hit multiplicity of 50 per track, as many as 5000 hits will be recorded on the 960 signal wires. A display of a Au on Au event with 79 found tracks is shown in Fig. 4. The position resolution of each individual hit is expected to be $\sigma_{XY} \approx 300$ μm and $\sigma_Z \approx 2$ cm. The actual resolution σ_{XY} approaches this value, however σ_Z is currently several times the design goal. In order to distinguish the many hits that occur on each wire every event, the signals are readout by FlashADCs (for more details see Section 4). The combination of this very high hit density into tracks from true particles poses a serious challenge to the tracking algorithms. Four independent routines have been developed to master this difficult task. The track resolution has been extensively studied by using the IQMD code [12] as an event generator and the GEANT package to simulate the detector response. These studies suggest that the resolution in determining the laboratory angles Θ and ϕ are $\sigma_\Theta = 6°$ and $\sigma_\phi = 0.6°$. The relative momentum resolution σ_{p_t}/p_t rises from 4% for $p_t < 0.5$ GeV/c to about

12% for $p_t = 2$ GeV/c. The specific energy loss (dE/dx) resolution is expected to be between 5-10%.

Particle identification is achieved by combining the specific energy loss with the momentum. The mean rate of energy loss is given by the Bethe-Bloch equation, which relates dE/dx to the velocity of the incoming particle. Thus, for a given momentum particles with different masses do not have the same dE/dx. This mass separation is demonstrated by the data in Fig. 5. In this figure the negatively charged particles

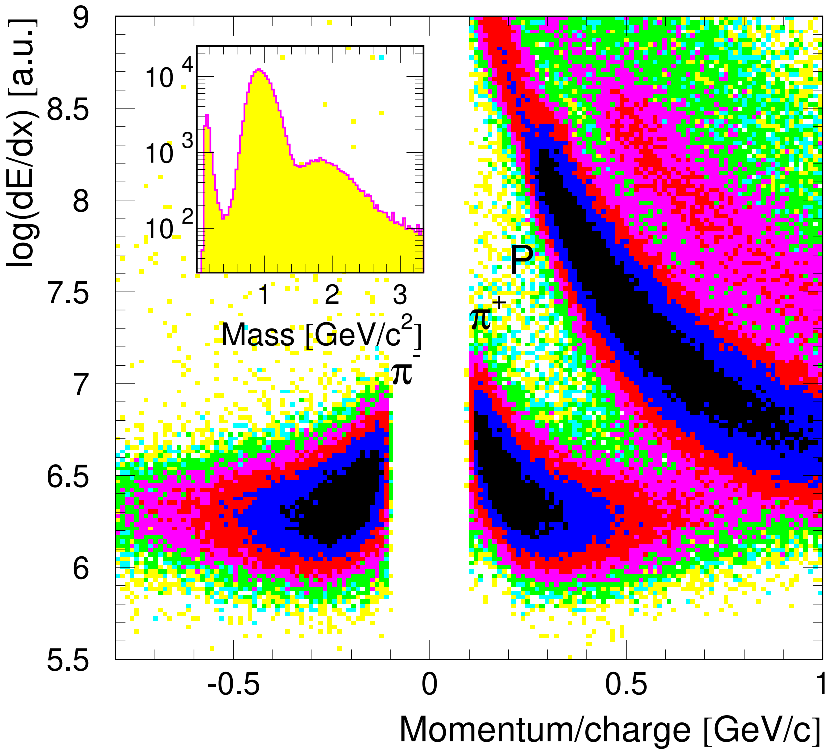

Figure 5: Specific energy loss as a function of particle momentum. Negatively charged particles are assigned a negative momentum. The insert contains a linearization of this data which was measured with the system 1.8 A·GeVNe on Al.

are displayed with negative momentum and the insert contains a linearization of this data. Near 0.4 GeV/c the pions traverse a minimum in dE/dx which rises with increasing momentum. Above 0.6 GeV/c the π^+ branch starts to vanish under the much more numerous protons. A linearization of these data is given in the insert.

The first major experiment with the second phase of FOPI was a study of charged pion production in the system Au on Au at 1.06 A·GeV. Analysis of this experiment is not complete, however some first results are available. The $\pi^\pm$ multiplicities are displayed in Fig. 6 as a function of the number of participants (A_{part}). A_{part} is a measure of the event centrality via a geometric model [13]. This figure also includes for comparison π^+ data from the KaoS [14] and π^0 data from the TAPS [9] collaborations at GSI. The pion multiplicities increase roughly linearly with A_{part} (increasing

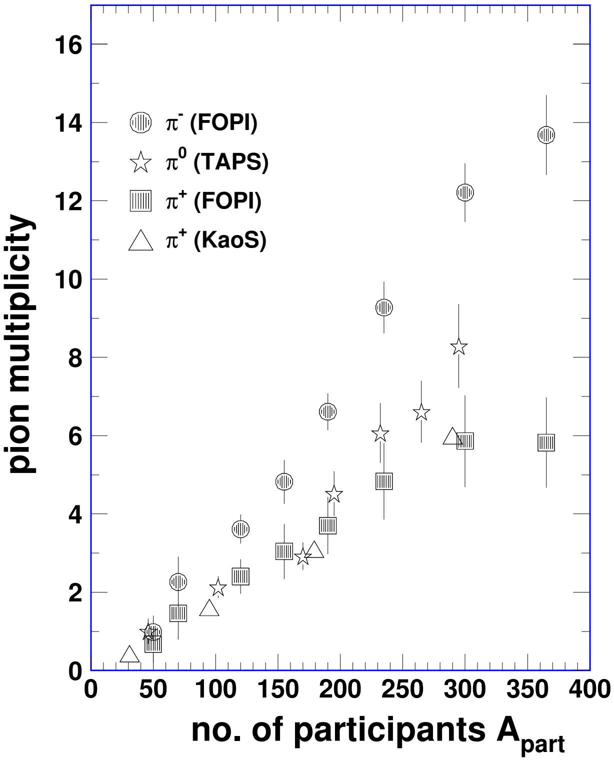

Figure 6: Compilation of the pion multiplicities as a function of the number of participating nucleons, measured by the KaoS, TAPS, and FOPI collaborations in the system Au + Au at 1 A·GeV.

centrality), and at large values of A_{part} the relative yield $M(\pi^-)/M(\pi^0)/M(\pi^+)$ are in agreement with the prediction (1.95/1.42/1.00) by the isobaric model [15].

4 Data Acquisition

Before proceeding to the partially completed third phase of FOPI, the current data acquisition system will be described here.

The FOPI data acquisition system is based on a variety of VME-type computers, all of which use processors from the Motorola 68000 family. A summary of the processors used is given in Table 1. The AEB is a CERN development for FASTBUS readout, while the CVI is a GSI construction for CAMAC readout. A schematic diagram of how these processors are combined for the full data acquisition system is given in Fig. 7.

The readout of an event in initiated by the production of a trigger signal. The

Name		*CPU*	*Memory*	*Op. Sys.*
ELTEC-Eurocom 5	E5	68020	1 MB	OS9
ELTEC-Eurocom 6	E6	68030	4 MB	OS9
ELTEC-Eurocom 7	E7	68040	4 MB	OS9
ALEPH event builder	AEB	68020	4 MB	OS9
CES FIC8230	FEP	68020	1 MB	Psos
GSI built CVI	CVI	68020	1 MB	Psos

Table 1: Overview of the processors used by the data acquisition.

trigger for a central event is produced when all the following conditions are coincident:

- valid start detector signal,
- high multiplicity in the Forward Wall,
- spill gate (beam on target), and
- not a test event (neither laser nor pulser fired).

This trigger signal must be produced within 300 ns of the event in order to set up the FASTBUS modules for digitalization and readout. The readout of the digitized data is signaled differently for the various detector components. The readout of the CAMAC and FASTBUS data (Forward Wall and Barrel) is controlled by the Triggerbus. The Triggerbus is a GSI designed, 16 bit bus which maintains a synchronization of the independent readout processors (CVI and AEB) and allows up to 15 different readout types to be handled. Depending upon the readout type, the AEB performs pedestal subtraction and zero suppression before copying its subevent to a dual-ported memory. The dead-time is reset only after all processors connected to the triggerbus are finished with the readout. On the other hand, the Flash-ADCs (FADC) run continuously with a frequency of 100 MHz and are stopped 7 μs after the selected interaction occurred.

After all possible Fast Clear option have time out the readout of the FADCs is triggered. The combined data flow from 960 wires read out on both sides each with 1024 FADC channels (8 bit) approaches 2 MB/event. This copious output demands frontend data reduction. More than a factor 10 reduction can be achieved by only reading out those channels with a signal larger than a software controlled threshold. Further reduction down to about 10-30 kB/evt is obtained by analyzing the signal on each wire and only recording the time and amplitude of each hit. To handel this online data reduction, each FADC is readout by an E5 (see Table 1) which distributes the data to a farm of 30 E7 processors and afterwards resets the deadtime. After the E7s finish calculating the reduced quantities, the hit information from all 6 VME

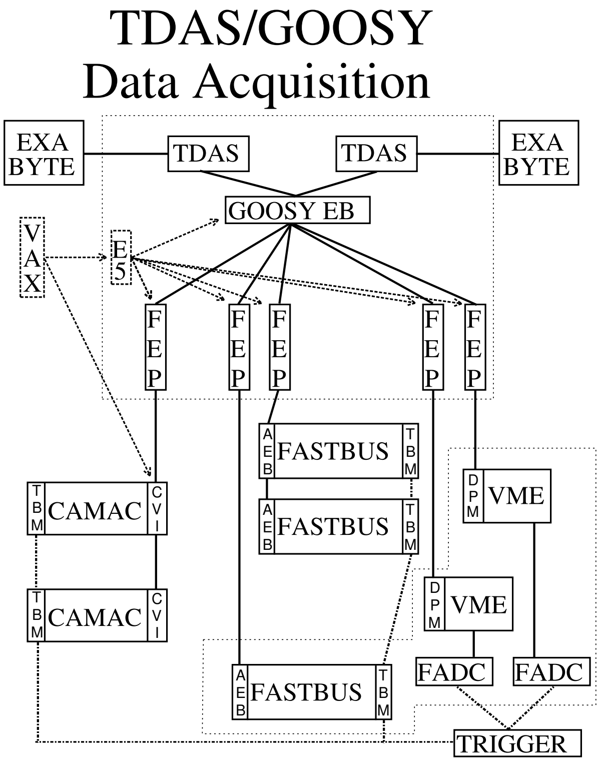

Figure 7: Overview of the FOPI data acquisition system.

crates is collected by other E7s into a subevent which is copied to a dual ported memory.

The ability of this system to process several subevents concurrently, demands that the subevents from the other detector components are stored (pipelined) until the full event can be assembled. The needed pipelining is achieved with the system GOOSY from GSI. For this task each subsystem is assigned its own front end processor (FEP) which collects the subevents from the dual ported memories and stores them in an internal queue. On another FIC -the Event Builder- all the subevents are combined and copied to TDAS. TDAS (Tenable Data Acquisition System) consists of three independent processes on an E6 that access a triple ring buffer as shown in Fig. 8. The GOOSY event buffers are copied from the Event Builder into the ring buffer by the TDASacquire process. Afterwards, the data are stored to a local exabyte tape drive with the Process TDASarchive. Online data analysis is organized by the process TDASaccessd. Upon receiving a request from a workstation for online data, a subprocess (TDASaccessdc) is spawned which copies the events over TCP/IP protocol to the workstation. Since not all events can be transferred, this process allows for a filter so only events with selected trigger type and/or specific subevent types need be copied. This process runs at low priority to inhibit contributions to

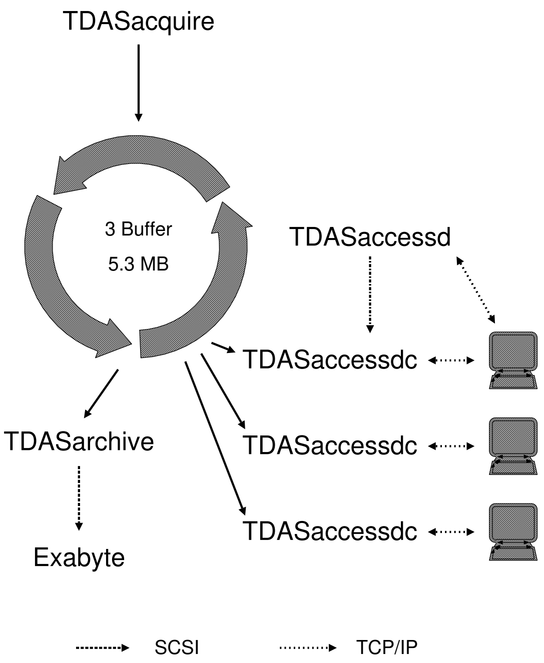

Figure 8: The TDAS data acquisition system.

the computer deadtime and is removed when the online analysis has terminated.

In order to enhance the data throughput, the spill structure delivered by the synchrotron accelerator (4-6 seconds of beam extraction per 10 s cycle) has been exploited. With a beam current of 10^5 particles/sec approximately 1.5-2 Mb/sec is produced. Because of the 50% duty cycle a taping capability of 0.8-1 Mb/sec is required. This taping rate is achieved by distributing the data between two E6s each running with a TDAS.

5 Barrel and HELITRON

Currently the final preparations are being made to install the remaining sub-systems of the completed FOPI facility. These include the Scintillator and Cherenkov Barrel which surrounds the CDC to improve its particle identification and the drift chamber HELITRON which enables isotope separation in the forward directions.

The Barrel consists of 180 individual detectors arranged in a cylindrical pattern with each aligned parallel to the beam axis. Each of these detectors contains a $240 \times 4 \times 3$ cm^3 plastic scintillator strip at a radius of 111 cm from the beam axis and a $100 \times 3 \times 3$ cm^3 water filled Cherenkov counter located directly behind the scintillator strip. The plastic strips cover the laboratory polar angular range $45° < \Theta_{lab} < 140°$ and almost the full azimuth with the exception of two 11° wide holes needed for the mechanical support of the CDC. The Barrel strips are readout with EMI9814B 2" photmultipliers. Because of the long length of these strips they must be readout on both sides in order to determine the quantities ToF, POS, and ΔE as is done for the Forward Wall. Depending upon the position and the amount of primary light the time resolution varies between $\sigma_t \approx 140 - 300$ ps. This corresponds to a position resolution of about $\sigma_z \approx 3$ cm. The Cherenkov counters cover the laboratory polar angular range $45° < \Theta_{lab} < 85°$. Amino G salt from Dubna has been added at a concentration of 55 mg/l as a wavelength shifter. Studies with cosmic μ^- and reaction products from the system 1.8 A·GeV Ne on Al indicate a mean of 8 photoelectrons produced by relativistic particles incident on the farthest point from the photomultiplier.

By combining the velocity measured in the Barrel with the momentum and energy loss from the CDC, an additional redundancy is achieved which improves the particle identification capabilities. Although the CDC can determine the sign of the fragment's charge (Z), the velocity measurement from the Barrel allows the magnitude to be extracted. For a given charge, the particle mass is uniquely determined by the momentum and velocity. A subset of the Barrel detectors have already been installed and tested with the reaction 1.93 A·GeV Ni on Ni. A plot of the momentum versus velocity of the $Z = +1$ reaction products from this test is shown in Fig. 9. Not only are lines from π^+, protons, deuterons, and tritons clearly visible in this

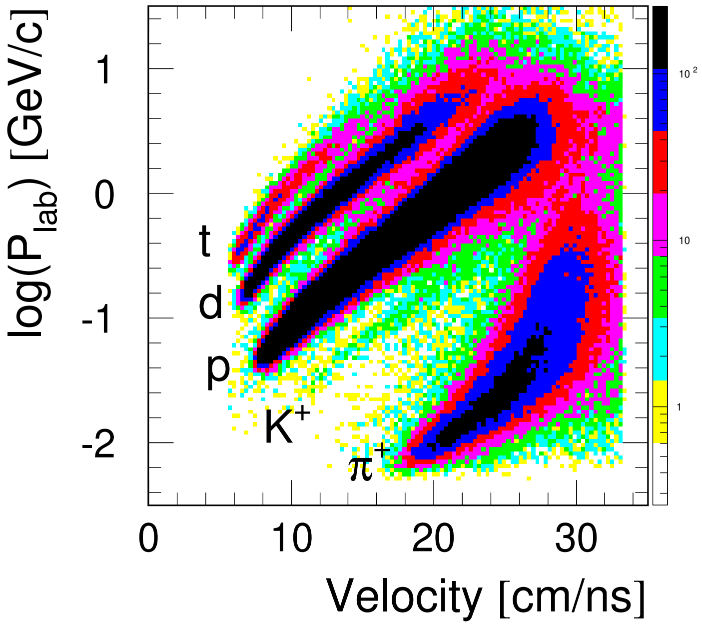

Figure 9: Momentum measured by the CDC plotted as a function of the velocity measured in the Barrel for $Z = +1$ particles.

figure, but also a distinct contribution from K^+ can be seen. By utilizing the Barrel, the upper limit for kaon identification can be raised to approximately 0.9 GeV/c from ~ 0.5 GeV/c for the CDC alone. A lower transverse momentum threshold (0.1 GeV/c) is determined by the minimum radius of curvature needed for the particles to reach the Barrel. By additionally employing the Cherenkov counters to suppress the proton yield, π^+-proton separation is achieved with these data to beyond 1.2 GeV/c.

The particle mass can be calculated with the following formula:

$$M = \frac{P}{\gamma\beta}.$$

Here P is the momentum, γ the relativistic contraction factor, and β the normalized velocity. Using this formula, the data in Fig. 9 with $P \leq 0.6$ GeV/c have been linearized and the results are shown in the mass spectra in Fig. 10. For the positively

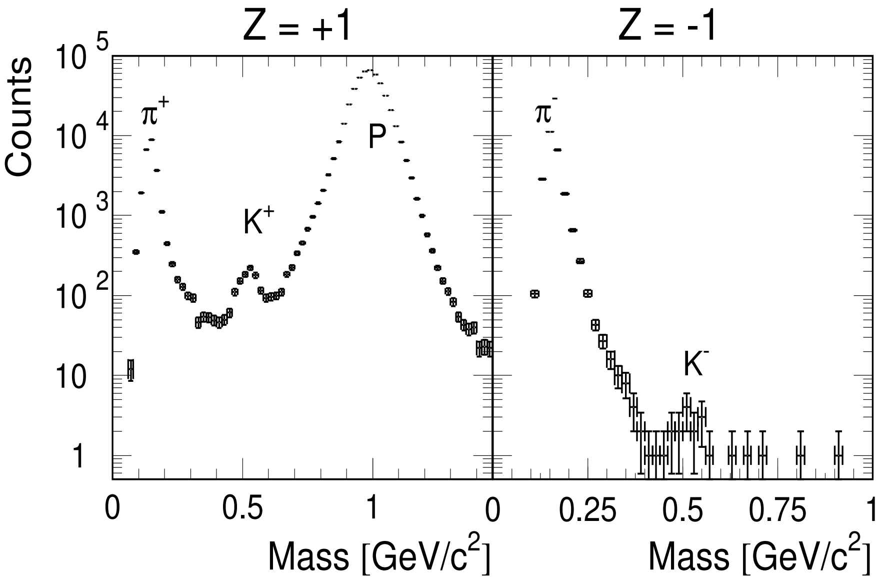

Figure 10: Reconstructed mass using the matched CDC-Barrel data for $p_{lab} < 0.6$ GeV/c for positively charged particles (a) and negatively charged particles (b).

charged particles a large peak is located near 0.5 GeV/c^2 which is associated to the K^+ meson. Above $P \sim 0.9$ GeV/c this peak vanishes due to the finite detector resolution. At lower momenta, the background is dominated by mismatched Barrel and CDC data. The mass spectrum of negatively charged particles ($P_{lab} < 0.6$ GeV/c) reveals, in addition to the π^- contribution, a statistically significant peak near 0.5 GeV/c^2 which is considered evidence of the antikaon signal.

In order to conserve strangeness, the K^+ must be coproduced with another strange particle; the reaction channel with the lowest threshold (1.6 GeV) is:

$$N + P \rightarrow N + \Lambda + K^+.$$

Since the Λ is neutral and decays with a lifetime $c \cdot \tau_0 = 7.9$ cm it can not be directly measured in the CDC. However, the products of its main decay channel ($\Lambda \rightarrow p\pi^-$, branching ratio 64%) can be readily detected by the CDC. The Λ is identified by calculating the invariant mass (M_{inv}) of all $p\pi^-$ pairs that intersect to form a secondary vertex away from the main event vertex as shown by the solid

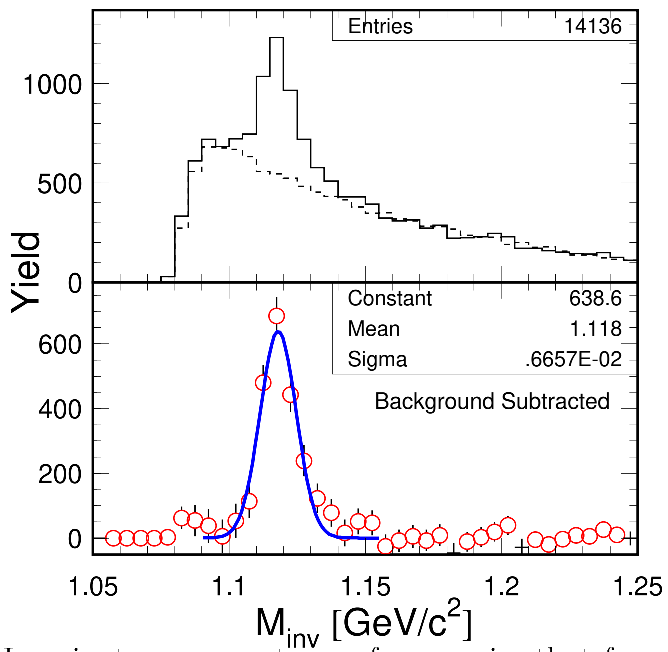

Figure 11: (a) Invariant mass spectrum of $p\pi^-$ pairs that form a secondary vertex more than 3 cm from the target (solid histogram). The mixed event background is denoted by the dashed histogram. (b) Λ baryon peak with a gaussian fit after background subtraction.

histogram in Fig. 11. In this figure a very pronounced peak is visible above the mixed event background which is marked by the dashed histogram. After background subtraction, a peak remains which is located at E_0 = 1.118 GeV/c^2 with a width σ = 6.7 MeV/c^2. The +2 MeV/c^2 systematic shift in M_{inv}, and the width of the peak can serve as a measure of the quality of the calibration currently employed. This shift and the width both decrease somewhat for secondary vertices even further away from the target. Within this data sample, there is approximately 1 Λ per 1000 central events recorded, while for peripheral events this ratio drops to 1:10^4. These counts rates are primarily determined by acceptance effects and will require detailed analysis to yield production probabilities.

The forward drift chamber HELITRON is currently in the final stages of preparation to be installed. The HELITRON will add isotope separation to the elements identified by the Forward Wall within the angular range $7° < \Theta_{lab} < 30°$. The HELITRON is subdivided into 24 sectors each containing 54 sense and 53 potential wires. All the individual wires are mounted radially, perpendicular to the beam axis. Within each sector the wires are mounted in planes parallel to the beam axis. The potential wires are made of 125 μm diameter CuBe, and the readout wires are 50 μm diameter NiCr with 1kΩ/m resistivity. The mechanical load on the wires was fixed at 3 N and 0.8 N respectively. An extension of the gas flow system of the CDC was undertaken to supply the HELITRON. In-beam tests, with only three sectors connected, were performed with the system Kr + Pb. During this test a considerable effort was required to reduce the level of external electromagnetic noise pick-up. First results from this test demonstrate the HELITRON's ability to discriminate the p,d,t isotopes.

6 Summary

This report describes the current status of the FOPI detector system which was designed to study central and semicentral heavy ion collisions in the 1 A·GeV regime. In the first phase the Forward Wall was constructed in 1990. The Wall covers the full azimuth within the polar angular range 1° to 30°. Via ΔE and ToF measurements the the charge and velocity of fragments up to $Z \sim 20$ is resolved. In a second construction phase a superconducting magnet and the CDC were installed in 1992. The CDC is a drift chamber of the jet type which measures the momentum and specific energy loss of reaction products over the full azimuth with Θ_{lab} between 30° and 150°. Currently the final completion of the FOPI system is being prepared with the commissioning of the Barrel and HELITRON planned for the beginning of 1995.

The existing components of the FOPI have been used in several experiments with symmetric projectile-target system. Furthermore, in-beam tests have been carried out on portions of the Barrel and HELITRON. The results of these test presented in this report show that the completed FOPI system is capable to perform a rich collection of sensitive measurements that may provide experimental constraints on various models of nuclear matter at high density and temperature.

References

[1] FOPI Collaboration, Technical Proposal: *GSI Report* **88-03** (1988).

[2] A. Gobbi et al.: *Nucl. Inst. Meth.* **A324** (1993), 156.

[3] J. P. Alard et al.: *Phys. Rev. Lett.* **69** (1992), 889.

[4] B. Kämpfer et al.: *Phys. Rev. C* **48** (1993), R955.

[5] C. Kuhn et al.: *Phys. Rev. C* **48** (1993), 1232.

[6] S. C. Jeong et al.: *Phys. Rev. Lett.* **72** (1994), 3468.

[7] Y. Leifels et al.: *Phys. Rev. Lett.* **71** (1993), 963.

[8] L. Venema et al.: *Phys. Rev. Lett.* **71** (1993), 835.

[9] O. Schwalb et al., *Phys. Lett.* **B321** (1994), 3650.

[10] F.-D. Berg et al., *Phys. Rev. Lett.* **72** (1994), 977.

[11] J. L. Ritman et al.: *Phys. Rev. Lett.* **70** (1993), 533.

[12] St.A. Bass et al.: *Phys. Rev. Lett.* **71** (1994), 1144.

[13] V. Metag: *Prog Part and Nucl Phys* **30** (1993), 75.

[14] D. Miśkowiec et al.: *Phys. Rev. Lett.***72** (1994), 3650.

[15] R. Stock et al.: *Phys. Rep.* **135** (1986), 259.

* The FOPI collaboration is comprised of members from the following institutes: INPE Bucharest, CRIP Budapest, LPC Clermont-Ferrand, GSI Darmstadt, Univ. Heidelberg, ITEP/KIAE Moscow, FZ Rossendorf, CRN Strasbourg, Univ. Warsaw, and RBI Zagreb.